Superresolving Multiphoton Interferences with Independent Light Sources

S. Oppel,[1,2] T. Büttner,[1] P. Kok,[3] and J. von Zanthier[1,2,*]

[1]Institut für Optik, Information und Photonik, Universität Erlangen-Nürnberg, 91058 Erlangen, Germany
[2]Erlangen Graduate School in Advanced Optical Technologies (SAOT), Universität Erlangen-Nürnberg, 91052 Erlangen, Germany
[3]Department of Physics and Astronomy, University of Sheffield, Sheffield S3 7RH, United Kingdom

(Received 18 May 2012; published 4 December 2012)

We propose to use multiphoton interferences from statistically independent light sources in combination with linear optical detection techniques to enhance the resolution in imaging. Experimental results with up to five independent thermal light sources confirm this approach to improve the spatial resolution. Since no involved quantum state preparation or detection is required, the experiment can be considered an extension of the Hanbury Brown–Twiss experiment for spatial intensity correlations of order $N > 2$.

DOI: 10.1103/PhysRevLett.109.233603 PACS numbers: 42.50.St, 03.65.Ta, 03.67.Ac, 42.50.Ex

Multiphoton interferences with indistinguishable photons from statistically independent light sources are at the focus of current research owing to their potential in quantum information processing [1,2], creating remote entanglement [3,4], and metrology [5–7]. The paradigmatic states for multiphoton interference are the highly entangled NOON states [8], which can be used to achieve increased resolution in spectroscopy, lithography, and interferometry [8–12]. However, multiphoton interferences from statistically independent emitters—either nonclassical or classical—can also lead to enhanced resolution in metrology and imaging [10,13–15]. So far, such interferences have been observed with maximally two independent emitters [10,16–26]. Here, we propose to use multiphoton interferences in a configuration that can be implemented with both classical and nonclassical independent sources to obtain spatial interference patterns equivalent to those of NOON states. Our scheme is an extension of the theoretical proposal of Ref. [15], which uses a different detection scheme and requires nonclassical sources. Experimental results with up to five independent thermal light sources confirm our approach to enhance the spatial resolution in imaging.

In the case of NOON states, the N-photon interference pattern can be written as [8]

$$I_N(\mathbf{x}) \propto \frac{1}{2}[1 + V_N \cos(N\mathbf{k}\mathbf{x})], \tag{1}$$

where N is the number of photons participating in the NOON state, V_N is the visibility, $\mathbf{k}$ is the difference vector between the wave vector $\mathbf{k}_1$ and $\mathbf{k}_2$ of the interfering light fields, and $\mathbf{x}$ is the position along the observation screen. An N-photon spatial interference pattern as in Eq. (1) can be used to enhance the resolution in interferometry and imaging. As known from Abbe, an image of an object is formed if the rays contributing to adjacent diffraction orders (e.g., 0, +1) in the diffraction plane are captured by the aperture $\mathcal{A}$ of the imaging device, since then all information of the object is contained in the diffraction pattern via Fourier transform [27]. For a grating with N slits and slit spacing d, this leads to a minimal resolvable slit separation $d_{\min} = \lambda/(2\mathcal{A})$, with an error $\Delta d_{\min} = \lambda/(4\mathcal{A})$ [27]. This limit can be overcome if the slowly oscillating terms in the diffraction pattern of the grating $I \propto 1 + \frac{2}{N}\sum_{\alpha=1}^{N-1}(N-\alpha)\cos(\alpha\delta)$ with $\delta = kd\sin\theta$ are suppressed such that only the modulation at the highest frequency $\cos[(N-1)\delta]$ prevails, containing all relevant parameters of the grating (N and d). Based on counting the number of peaks M across $\mathcal{A}$ in the NOON-like interference pattern $1 + V_N\cos[(N-1)\delta]$, we obtain $2\pi M = 2\mathcal{A}(N-1)kd$. From this, assuming a signal to noise ratio such that $\Delta M < 1/2$, we derive the slit separation d and its error Δd as

$$\begin{aligned} d &= \frac{M\lambda}{2\mathcal{A}(N-1)}, \\ \Delta d &= \Delta M \left|\frac{\partial M}{\partial d}\right|^{-1} < \frac{\lambda}{4\mathcal{A}(N-1)}. \end{aligned} \tag{2}$$

According to Eq. (2), for $N - 1 > M \geq 1$ the pattern conveys information about source details that are smaller than the Abbe limit.

A superresolving N-photon interference pattern as in Eq. (1) can be obtained with statistically independent light sources by using linear optical detection techniques. Consider N independent emitters at $\mathbf{R}_\alpha$ ($\alpha = A, B, \ldots$) along a chain with equal spacing d (see Fig. 1), and place $N-1$ detectors in a semicircle in the far field around the sources at specific *magic angles* which will be defined below. The emitters are assumed to emit photons of identical frequency and polarization and may be single photon emitters (SPE) or classical thermal light sources (TLS). Moving another detector along the semicircle and postselecting on simultaneous single photon detection events in each of the N detectors will produce an interference pattern I_{N-1} as in Eq. (1), where $\mathcal{A}$ is defined with respect to the one detector which is scanned. To see this, we recall that the N-photon interference pattern is proportional to the (normally ordered) N-point intensity correlation function

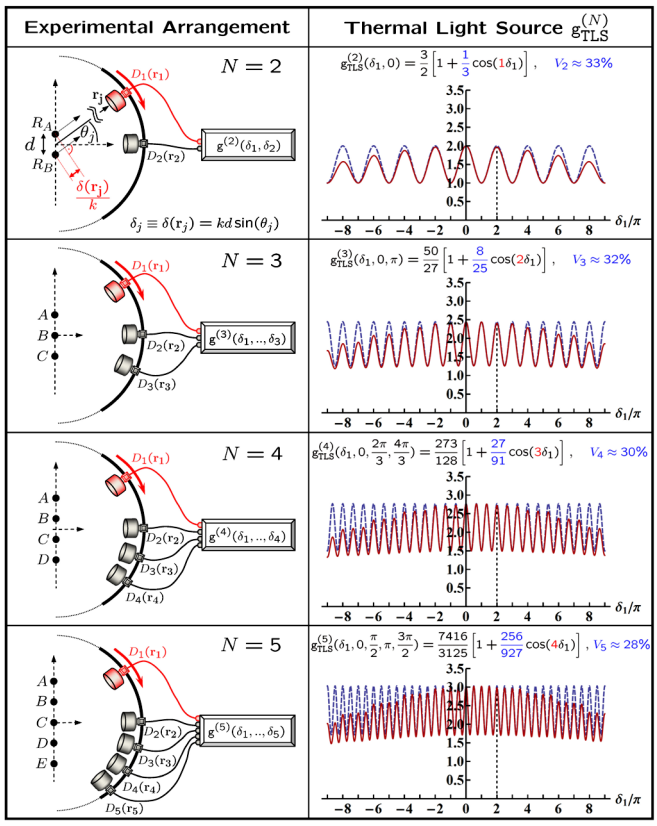

FIG. 1 (color online). Left column: Scheme for measuring $g^{(N)}(\delta_1,\ldots,\delta_N)$ for $N = 2,\ldots,5$ equidistant independent emitters located at $\mathbf{R}_\alpha$ ($\alpha = A, B, \ldots$). N detectors D_j at $\mathbf{r}_j$ ($j = 1,\ldots,N$) measure N emitted photons in the far field within a joint detection time interval. Right column: Theoretical plots of $g^{(N)}(\delta_1,\ldots,\delta_N)$ for $N = 2,\ldots,5$ TLS for the indicated fixed detector positions δ_j ($j = 2,\ldots,N$) as a function of δ_1 for pointlike emitters (dashed blue curve) and extended sources (solid red curve).

$$g^{(N)}(\mathbf{r}_1,\ldots,\mathbf{r}_N) \equiv \frac{\langle :\prod_{j=1}^{N}\hat{E}^{(-)}(\mathbf{r}_j)\hat{E}^{(+)}(\mathbf{r}_j):\rangle}{\prod_{j=1}^{N}\langle\hat{E}^{(-)}(\mathbf{r}_j)\hat{E}^{(+)}(\mathbf{r}_j)\rangle}, \quad (3)$$

where $\langle\cdot\rangle$ denotes the quantum mechanical expectation value and $\hat{E}^{(+)}(\mathbf{r})$ and $\hat{E}^{(-)}(\mathbf{r})$ are the positive and negative frequency parts of the total electric field operator at position $\mathbf{r}$, respectively. Here, $\hat{E}^{(+)}(\mathbf{r}_j) \propto \sum_\alpha \hat{a}_\alpha e^{ikr_{\alpha j}}$, where $\hat{a}_\alpha$ is the annihilation operator of a photon emitted by source α and $r_{\alpha j} = |\mathbf{R}_\alpha - \mathbf{r}_j|$ is the distance between the source α and the detector D_j. Since the emitters are uncorrelated, the state of the field is given by $\rho = \otimes_\alpha \rho_\alpha$, where $\rho_\alpha = \sum_n P_\alpha(n)|n\rangle\langle n|$, with $P_\alpha(n)$ the photon number distribution for the modes originating from source α.

With the $N-1$ detectors at the magic positions, given in terms of phases $\delta_j = kd\sin(\theta_j)$ by

$$\delta_j = 2\pi(j-2)/(N-1), \qquad j = 2,\ldots,N, \quad (4)$$

the second- and third-order correlation functions for two and three TLS reduce to

$$g^{(2)}_{\mathrm{TLS}}(\delta_1,0) = \frac{3}{2}\left[1+\frac{1}{3}\cos(\delta_1)\right], \quad (5)$$

$$g^{(3)}_{\mathrm{TLS}}(\delta_1,0,\pi) = \frac{50}{27}\left[1+\frac{8}{25}\cos(2\delta_1)\right], \quad (6)$$

whereas the Nth-order correlation function is given by

$$g^{(N)}_{\mathrm{TLS}}(\delta_1) \propto 1 + V_N\cos[(N-1)\delta_1]. \quad (7)$$

Because of the possibility of multiple photons originating from the same source, the visibility V_N of $g^{(N)}_{\mathrm{TLS}}$ is smaller than 100%, gently decreasing to $V_{10} \approx 21\%$ for $N = 10$. In the case of SPE, the second- and third-order correlation functions take the form [28]

$$g^{(2)}_{\mathrm{SPE}}(\delta_1,0) = \frac{1}{2}[1+\cos(\delta_1)], \quad (8)$$

$$g^{(3)}_{\mathrm{SPE}}\left(\delta_1,\frac{3\pi}{4},\frac{5\pi}{4}\right) = \frac{4}{27}[1+\cos(2\delta_1)], \quad (9)$$

whereas the Nth-order correlation function reads

$$g^{(N)}_{\mathrm{SPE}}(\delta_1) \propto 1 + \cos[(N-1)\delta_1]. \quad (10)$$

Here, the visibility of $g^{(N)}_{\mathrm{SPE}}$ remains 100% for any N. In all cases the superresolving NOON-like modulation of $g^{(N)}(\delta_1)$ as in I_{N-1} of Eq. (1) is clearly visible [29]. However, note that the type of interference is fundamentally different from that of NOON states: In our case, the $(N-1)$-fold modulation relies on the suppression of lower spatial frequencies of the source, whereas in the case of NOON states it is linked to the reduced de Broglie wavelength of the state [8,23].

By changing for different N the angles $\theta_2,\ldots,\theta_N$ of detectors $D_2,\ldots,D_N$ such that the relative phase relation for the magic positions $\delta_j - \delta_{j-1} = 2\pi/(N-1)$, $j = 3,\ldots,N$, is fulfilled, one can monitor the interference pattern $g^{(N)}_{\mathrm{TLS}}(\delta_1)$ until the pure sinusoidal modulation as in I_{N-1} of Eq. (1) appears. In this case the number of detectors equals the number of slits, which determines N. The sought-after slit separation d can then be derived from the δ_j via $d = \lambda/\{(N-1)[\sin(\theta_j) - \sin(\theta_{j-1})]\}$. With this approach it is possible to determine N and d independently. For $N = 2,\ldots,5$ independent TLS, the calculated interference signals $g^{(N)}_{\mathrm{TLS}}(\delta_1)$ at the magic positions are displayed in Fig. 1, together with their exact analytical expressions.

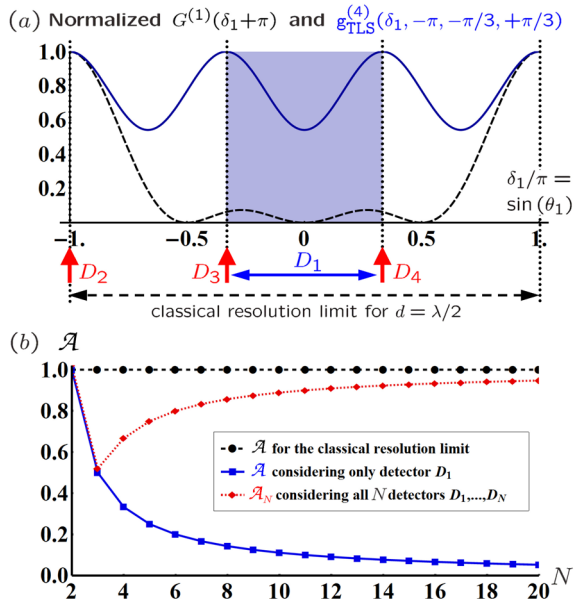

FIG. 2 (color online). (a) $g^{(4)}_{TLS}(\delta_1)$ for $N = 4$ independent TLS (solid blue curve) with detectors D_2, D_3, and D_4 at the magic angles $\delta_2 = -\pi$, $\delta_3 = -\pi/3$, $\delta_4 = +\pi/3$, and $G^{(1)}(\delta_1 + \pi)$ for a coherently illuminated grating with $N = 4$ slits (dashed black curve) in the case of a source or slit separation $d = \lambda/2$. The angular range required by detector D_1 to scan from one to the next principal maximum is indicated for $g^{(4)}_{TLS}(\delta_1)$ by a horizontal solid blue arrow and for $G^{(1)}(\delta_1 + \pi)$ by a horizontal dashed black arrow. The latter is the angular range required by the classical Abbe limit. (b) Numerical apertures required by the classical Abbe limit (dashed black curve), and by the proposed scheme for detector D_1 alone (solid blue curve) and for all N detectors (dotted red curve) to obtain structural information about a grating with N slits and slit separation $d = \lambda/2$.

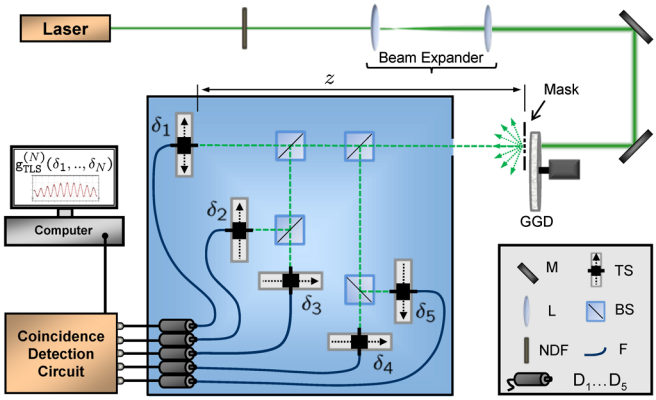

FIG. 3 (color online). Experimental setup for measuring $g^{(N)}_{TLS}(\delta_1)$. For details, see the text. GGD, ground glass disk; M, mirror; L, lens; NDF, neutral density filter; TS, translation stage with fiber mount; BS, beam splitter; F, multimode fiber; $D_1 \ldots D_5$, photomultiplier modules.

Note that the angular range $\mathcal{A}_N = \sin[(\theta_N - \theta_2)/2]$ required by all N detectors for $N > 2$ TLS is larger than the aperture $\mathcal{A}$ needed for detector D_1 alone. For a slit separation of $d = \lambda/2$, this is shown in Fig. 2. However, one can see from the figure that $\mathcal{A}_N$ always remains smaller than the aperture associated with the classical Abbe limit. Moreover, there is some flexibility in placing the $N - 1$ fixed detectors, for example, besides or behind the investigated object (assuming 4π emission), since the required values for the relative phase relations of the magic positions are valid modulo 2π. The dotted red curve representing $\mathcal{A}_N = \sin[(\theta_N - \theta_2)/2]$ in Fig. 2(b) does not take into account this flexibility.

The experimental setup used to measure $g^{(N)}_{TLS}(\delta_1)$ with up to $N = 5$ is shown in Fig. 3. To realize the N independent TLS, opaque masks with N identical slits of width $a = 25$ μm and separation $d = 250$ μm are illuminated by pseudothermal light originating from a linearly polarized frequency-doubled Nd:YAG laser at $\lambda = 532$ nm scattered by a rotating ground glass disk [30]. The large number of time-dependent speckles, produced by the stochastically interfering waves scattered from the granular surface of the disk, acts within a given slit as many independent pointlike subsources equivalent to an ordinary spatial incoherent thermal source [31]. To prove the thermal statistics of the TLS we measured the autocorrelation function $g^{(2)}(\tau)$ and verified that $g^{(2)}(\tau = 0) = 2.00(5)$ [13]. The coherence time of the pseudothermal light sources depends on the rotational speed of the disk [31] and was chosen to $\tau_c \approx 100$ μs so that a commercial coincident detection circuit could be used. The light from the masks is split by 50/50 nonpolarizing beam splitters and collected at a distance $z \approx 1$ m behind the glass disk by N laterally displaceable fiber tips of core diameter 50 μm, guiding the light to N single photon detectors. The output pulses of the photon detectors are then fed into a coincidence detection circuit. In the experiment the single photon counting rates for $g^{(2)}_{TLS}$, $g^{(3)}_{TLS}$, $g^{(4)}_{TLS}$, and $g^{(5)}_{TLS}$ correspond typically to 100–350 kHz. With joint detection time windows of 50, 410, 410, and 850 ns (ensuring the single photon counting regime) and taking into account the thermal photon statistics as well as varying quantum efficiencies of the different detectors, this leads to averaged N-fold coincidence rates of 1500, 1500, 400, and 300 Hz, respectively. Note that the $g^{(N)}_{TLS}(\delta_1)$ display the calculated interference signals only if the N photons are measured within their coherence time [13].

The experimental results for $g^{(2)}_{TLS}(\delta_1), \ldots, g^{(5)}_{TLS}(\delta_1)$ are shown in Fig. 4. The measured curves are in excellent agreement with the theoretical prediction if one takes into account the finite width of the slits [see red solid lines in Figs. 1 and 4(b)–4(e)]. The small deviations between the experimental results and the theoretical curves for $g^{(4)}_{TLS}$ and $g^{(5)}_{TLS}$ are mostly due to a slight misalignment of the detector positions from the required magic values. The deviations between $V^{(e)}_N$ and V_N towards higher N are mainly due to increased dead time effects arising from larger joint

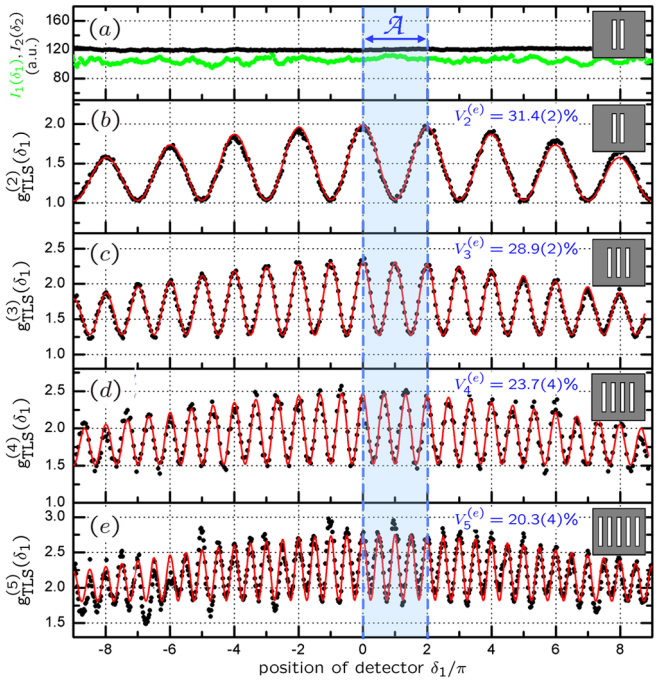

FIG. 4 (color online). Experimental results: (a) Measurement of average intensities I_1 and I_2 at detectors D_1 and D_2 alone (with D_1 scanned and D_2 kept constant), demonstrating that the pseudothermal light used is spatially incoherent in first order of the intensity. (b)–(e) Measurement of $g^{(N)}_{\mathrm{TLS}}(\delta_1)$ in the case of $N = 2, \ldots, 5$ TLS for $\delta_2, \ldots, \delta_N$ at the magic positions. Solid red curves correspond to a theoretical fit taking into account the finite width of the slits. The only fitting parameters are the slit separation d, the slit width a, and the visibility $V_N^{(e)}$. The experimentally obtained visibilities $V_N^{(e)}$ can be compared with the theoretical values V_N in Fig. 1.

detection time windows and higher single photon counting rates at the N detectors. From the figure it can be seen that the measured curves for $g^{(3)}_{\mathrm{TLS}}(\delta_1)$, $g^{(4)}_{\mathrm{TLS}}(\delta_1)$, and $g^{(5)}_{\mathrm{TLS}}(\delta_1)$ display a doubled ($2\delta_1$), tripled ($3\delta_1$), and quadrupled ($4\delta_1$) modulation frequency with respect to $g^{(2)}_{\mathrm{TLS}}(\delta_1, 0)$ and $g^{(2)}_{\mathrm{SPE}}(\delta_1, 0)$ [see Eqs. (5) and (8)]. This means that for a given aperture $\mathcal{A}$ (indicated in Fig. 4) $g^{(5)}_{\mathrm{TLS}}(\delta_1)$ exhibits 4 times more oscillations than $g^{(2)}_{\mathrm{TLS}}(\delta_1)$. According to Eq. (2), this beats the classical Abbe limit for Δd by a factor of 4.

In conclusion, we experimentally demonstrated spatial multiphoton interference patterns displaying superresolution with up to five statistically independent light sources by using linear optical detection techniques. For $N > 2$, these experiments achieve a higher resolution than the classical Abbe limit for imaging the light source. In the case of N SPE, we showed theoretically that the interference pattern obtained is identical to the one generated by NOON states with $N - 1$ photons, although the types of interference are fundamentally different [23]. Using N TLS leads to the same NOON-like modulation, although with a reduced visibility. Unlike for NOON states, our technique requires neither special quantum tailoring of light nor N-photon absorbing media, as it relies on single photon detection only. As intensity correlations of order $N > 2$ are used to improve the spatial resolution in imaging, it can be regarded an extension of the Hanbury Brown–Twiss experiment, one of the fundamental measurement techniques in quantum optics. The natural low light requirements suggest that the technique has potential applications for improved imaging of faint star clusters and *in vivo* biological samples.

The authors thank I. Harder for the fabrication of the masks and G. S. Agarwal, F. Schmidt-Kaler, A. Ramsay, A. Maser, U. Schilling, and R. Wiegner for critical discussions. The authors gratefully acknowledge funding by the Universitätsbund Erlangen-Nürnberg e.V., the Erlangen Graduate School in Advanced Optical Technologies (SAOT) by the German Research Foundation (DFG) in the framework of the German excellence initiative and the United Kingdom Engineering and Physical Sciences Research Council. S. O. thanks the Elite Network of Bavaria for financial support.

*Joachim.vonZanthier@physik.uni-erlangen.de

[1] E. Knill, R. Laflamme, and G. J. Milburn, Nature (London) **409**, 46 (2001).
[2] P. Kok and B. W. Lovett, *Introduction to Optical Quantum Information Processing* (Cambridge University Press, Cambridge, England, 2010).
[3] D. L. Moehring, P. Maunz, S. Olmschenk, K. C. Younge, D. N. Matsukevich, L.-M. Duan, and C. Monroe, Nature (London) **449**, 68 (2007).
[4] S. Olmschenk, D. N. Matsukevich, P. Maunz, D. Hayes, L.-M. Duan, and C. Monroe, Science **323**, 486 (2009).
[5] Y. Shih, *Advances in Laser & Electro Optics*, edited by N. Costa and A. Cartaxo (InTech, Vukovar, 2010).
[6] B. I. Erkmen and J. H. Shapiro, Adv. Opt. Photon. **2**, 405 (2010).
[7] V. Giovannetti, S. Lloyd, and L. Maccone, Nat. Photonics **5**, 222 (2011).
[8] A. N. Boto, P. Kok, D. S. Abrams, S. L. Braunstein, C. P. Williams, and J. P. Dowling, Phys. Rev. Lett. **85**, 2733 (2000).
[9] D. Leibfried M. D. Barrett, T. Schaetz, J. Britton, J. Chiaverini, W. M. Itano, J. D. Jost, C. Langer, and D. J. Wineland, Science **304**, 1476 (2004).
[10] M. D'Angelo, M. V. Chekhova, and Y. Shih, Phys. Rev. Lett. **87**, 013602 (2001).
[11] P. Walther, J.-W. Pan, M. Aspelmeyer, R. Ursin, S. Gasparoni, and A. Zeilinger, Nature (London) **429**, 158 (2004).
[12] M. W. Mitchell, J. S. Lundeen, and A. M. Steinberg, Nature (London) **429**, 161 (2004).
[13] R. Hanbury Brown and R. Q. Twiss, Nature (London) **177**, 27 (1956).
[14] A. Muthukrishnan, M. O. Scully, and M. S. Zubairy, J. Opt. B **6**, S575 (2004).

[15] C. Thiel, T. Bastin, J. Martin, E. Solano, J. von Zanthier, and G. S. Agarwal, Phys. Rev. Lett. **99**, 133603 (2007).
[16] R. Hanbury Brown, *The Intensity Interferometer* (Taylor & Francis, London, 1974).
[17] R. Kaltenbaek, B. Blauensteiner, M. Żukowski, M. Aspelmeyer, and A. Zeilinger, Phys. Rev. Lett. **96**, 240502 (2006).
[18] J. Beugnon, M. P. A. Jones, J. Dingjan, B. Darquié, G. Messin, A. Browaeys, and P. Grangier, Nature (London) **440**, 779 (2006).
[19] P. Maunz, D. L. Moehring, S. Olmschenk, K. C. Younge, D. N. Matsukevich, and C. Monroe, Nat. Phys. **3**, 538 (2007).
[20] R. Lettow, Y. L. A. Rezus, A. Renn, G. Zumofen, E. Ikonen, S. Götzinger, and V. Sandoghdar, Phys. Rev. Lett. **104**, 123605 (2010).
[21] K. Sanaka, A. Pawlis, T. D. Ladd, K. Lischka, and Y. Yamamoto, Phys. Rev. Lett. **103**, 053601 (2009).
[22] E. B. Flagg, A. Muller, S. V. Polyakov, A. Ling, A. Migdall, and G. S. Solomon, Phys. Rev. Lett. **104**, 137401 (2010).
[23] I. N. Agafonov, M. V. Chekhova, T. Sh. Iskhakov, and A. N. Penin, Phys. Rev. A **77**, 053801 (2008).
[24] I. N. Agafonov, M. V. Chekhova, T. Sh. Iskhakov, and L.-A. Wu, J. Mod. Opt. **56**, 422 (2009).
[25] Y. Zhou, J. Simon, J. Liu, and Y. Shih, Phys. Rev. A **81**, 043831 (2010).
[26] H. Bernien, L. Childress, L. Robledo, M. Markham, D. Twitchen, and R. Hanson, Phys. Rev. Lett. **108**, 043604 (2012).
[27] M. Born and E. Wolf, *Principle of Optics* (Cambridge University Press, Cambridge, England, 1998).
[28] For even numbers of SPE, the magic positions are given by Eq. (4); for odd numbers, the magic positions have been derived numerically.
[29] Note that to obtain a NOON-like modulation of $g^{(N)}(\delta_1)$ as in I_{N-1} of Eq. (1) in the case of SPE it is mandatory that the number of emitters equals the number of detectors; for TLS this can be obtained also by using more detectors than emitters.
[30] M. Rousseau, J. Opt. Soc. Am. **61**, 1307 (1971).
[31] L. E. Estes, L. M. Narducci, and R. A. Tuft, J. Opt. Soc. Am. **61**, 1301 (1971).